scientific reports

Check for updates

OPEN

Effect assessment for the interaction between shaking table and eccentric load

Juke Wang[1], Aiwen Liu[1,4], Xiaojun Li[2]✉, Zhenghua Zhou[3,4], Su Chen[2,4] & Jinbao Ji[2]

Electro-hydraulic shaking table is an essential experimental apparatus to evaluate structural performance under actual vibration condition. The control-structure interaction (CSI) between shaking table and eccentric load has lately received considerable attention for causing the accuracy degradation of shaking table test. At present, the research gap of the influence of the eccentricity of load on the CSI makes it challenging to find the CSI effects. And an effect assessment is yet to be proposed to evaluate the CSI effects, which has impeded the development of test technology. To overcome those theoretical bottlenecks, in this research, an analytical transfer function matrix of shaking table and eccentric load is established to analyze the CSI effects. The analysis is conducted under such conditions as different mass ratio (MR), moment of inertia ratio (IR), and eccentric distance ratio (ER) conditions. Through the analysis, the role of the ER is identified, the sensitivities of the MR, IR, and ER to the transfer function matrix are revealed, and the CSI effects are found. Furthermore, a novelty effect assessment is proposed to appraise whether the CSI effects can be ignored in shaking table test. And the visualization expression of the effect assessment is obtained for convenient application.

Electro-hydraulic shaking table is one of the most important pieces of equipment for replicating actual vibration conditions in various applications, including biomedical and geological researches[1–3], engineering seismic research works[4–6], aerospace vibration tests[7,8], and vehicle road simulations[9,10], etc. In the context of shaking table test, the control-structure interaction (CSI)[11–13] is the dynamic coupling between shaking table and load (that is the test structure model) (Fig. 1a,b). Due to the effects of the CSI, the control accuracy of shaking table and the accuracy of the response of load decrease to a great extent under some conditions[14–16]. Faced with these decreases, many researchers have taken shaking table and centrosymmetric load as research objects, and then established the models of shaking table and load (MST) and the other models (Fig. 1c). Based on the established models, the analysis of the CSI effects has been conducted with respect to two aspects: shaking table characteristics and structural (load) characteristics.

From the aspects of load characteristics, many researchers have analyzed the effects of mass, damping ratio, frequency rigidity and flexibility, the physical realization of damping and stiffness, degrees of freedom, and nonlinearity on the MST (Fig. 1d). Blondet and Esparza[17] analyzed the CSI effects on the MST under different MR, structure damping ratio, and structure frequency. The analysis showed that at the frequency of structure and its surrounding frequency band, the CSI effects increases with the MR and structure frequency, and decreases with structure damping ratio. Wang et al.[18] investigated the sensitivity of different test structure characteristics to the MST. The investigation revealed that structure frequency has the greatest influence on the MST, followed by structure damping ratio, and the MR is the smallest. Considering the dynamic coupling between base, platform, and structure, Conte and Trombetti[19,20] conducted simulation analysis and experimental verification to analyze their effects on the MST. The research came to a conclusion that base has slight impact on the MST, but structure exerts significant influence on the MST. Furthermore, the research revealed that structure frequency becomes the second resonance frequency of whole system, and rigid load decreases the resonance peak of oil column frequency. According to the physical realization of damping and stiffness, Conte and Trombetti[20] and Chen[21] improved the modeling accuracy of shaking table and structure. The improvement proved that the construction mode of damping/stiffness have an effect on the MST. Huang[22] studied the CSI effect between single degree of freedom structure and shaking table. The study demonstrated the MST has a resonance peak at the frequency

[1]Institute of Geophysics, China Earthquake Administration, Beijing 100081, China. [2]Beijing Key Laboratory of Earthquake Engineering and Structural Retrofit, Beijing University of Technology, Beijing 100124, China. [3]School of Transportation Engineering, Nanjing Tech University, Nanjing 211816, China. [4]These authors contributed equally: Aiwen Liu, Zhenghua Zhou and Su Chen. ✉email: beerli@vip.sina.com

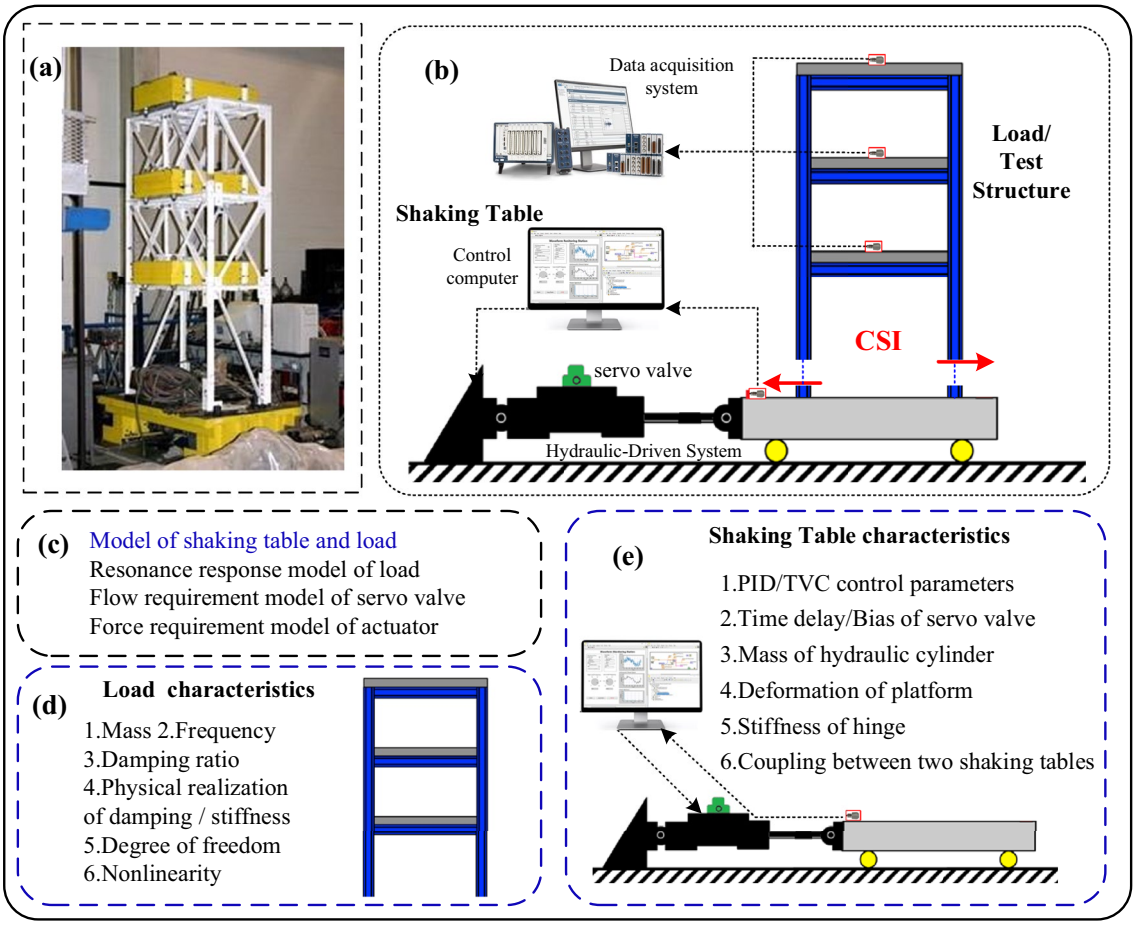

Figure 1. Analysis of the CSI effects. (**a**) Diagram of the shaking table and load, (**b**) dynamic coupling-CSI, (**c**) different Models, (**d**) different load characteristics, and (**e**) different shaking table characteristics.

of structure, and the resonance peak affects the control performance of shaking table. Tang et al.[23] analyzed the CSI effects between shaking table and multi degree of freedom structure. The analysis revealed that the CSI exert effects on the MST at the previous natural frequency of structure. Guo et al.[24] analyzed the CSI effects on shaking table tests. The analysis showed that the nonlinearity of test structure has great impact on the MST and the control accuracy of the shaking table decreases.

From the aspects of shaking table characteristics, many scholars have analyzed the effects of control parameters, the time delay and the bias of servo valve, the stiffness of hinge, the mass of hydraulic cylinder, the deformation of platform, and the coupling between two shaking tables on the MST (Fig. 1e). Trombetti et al.[20] studied the sensitivities of control gain (PID control parameter, feedforward gain, and differential pressure control gain) and servo valve delay to the MST. The study revealed that the control gain and the delay of servo valve have significant impact on the MST. Li et al.[25] analyzed the stability of the MST under different TVC parameters. The analysis showed that better system stability can be obtained with the no-load TVC control parameters. The influences of mechanical installation error, displacement measurement error, and bias of servo valve on the MST were considered in a study by Zhang[26]. The study shows the MST is only related to the bias of servo valve. And the CSI effects increases with the bias of servo valve. Yan studied the influence of the mass of exciter on the MST and found that the CSI effects increase with the mass of exciter[27]. The influence of the stiffness of hinge on the MST is investigated by Xie[28]. The investigation suggests that the stiffness hinge should be increased as much as possible. Maoult et al.[29] adopted finite element modeling to investigate the phenomenon of structural frequency reduction in large-scale shaking table experiments. The investigation demonstrated that the deformation of shaking table is the main reason for the CSI effects. In other words, the deformation of shaking table is one of the factors that affect the MST. Wang[30] and Li[31] studied the CSI effect between dual shaking tables and structure. The study revealed that the coupling effect between the two shaking tables have significant impact on the MST at the frequency of structure and its surrounding frequency band.

Additionally, Wang et al.[32] analyzed the CSI effects on the flow requirement model of servo valve, the force requirement model of exciter, and the resonance response model of load. The analysis was conducted under different load mass, the damping ratio of load, and the frequency of load conditions. The analysis shows the CSI must be considered in designing of the actuator force of actuator, and the flow requirement of servo valve can be achieved without considering the CSI when the flow requirement in the low-frequency band is satisfied.

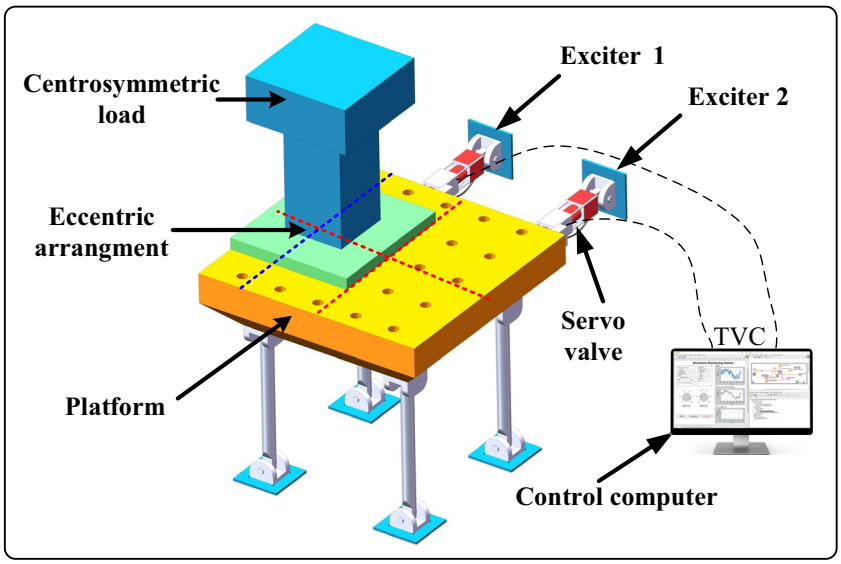

Figure 2. Schematic diagram of the shaking table and eccentric load.

To date, researchers have conducted studies that are limited to analyzing the CSI effects between shaking table and centrosymmetric load. However, most of loads in shaking table test are non-centrosymmetric. The CSI increases greatly when an eccentric load is loaded on shaking table in the studies of Zhao et al[14,33]. Guo et al.[34] investigated the influence of different test structures on the control performance of shaking table, and the investigation showed that the control performance is greatly affected by the eccentricity of test structure. Therefore, it is necessary to study the CSI effects between shaking table and eccentric load. Moreover, the eccentric degree of load and the moment of inertia of load are important characteristics that have not been analyzed in previous studies. Furthermore, no effect assessment has been proposed to evaluate the CSI effects, and thus, the existing research needs to be further expanded.

In this study, an analytical transfer function matrix is established to analyze the CSI effects between twin-axes shaking table and eccentric load. Based on the transfer function matrix, an in-depth investigation is conducted under different MR, IR, and ER conditions. The sensitivities of the MR, the IR, and the ER to the transfer function matrix, as well as the influence frequency range and the influence trend of the CSI effects, are found in the investigation. Furthermore, a novelty effect assessment is proposed to appraise the CSI effects.

Analytical modeling

The schematic diagram of the twin-axes shaking table and eccentric load is presented in Fig. 2. It can be seen from Fig. 2 that the shaking table is driven by two exciters in horizontal direction, and a centrosymmetric load is loaded on the platform eccentrically. It is worth noting that the ingenious arrangement can simulate the condition that an eccentric load is loaded on the platform to a great extent. Meanwhile, the analytical modeling process of the transfer function matrix is greatly simplified.

The transfer function matrix is established according to the modular method presented in Fig. 3. The method divides the shaking table and eccentric load into three main sub-models, including the dynamic model, the hydraulic-driven model, and the TVC model, which are shown in Fig. 3a. It should be noted that the components and the physical characteristics of the three sub-models are comprehensively considered in the modeling process. Detailed explanations of symbols are given in the following description of the modeling process, and the values of the parameters are listed in Table S1 in the Supplementary Materials.

Dynamic system modeling. The dynamic model is the motion mechanism part of the shaking table and eccentric load. Without regard to the stiffness and the damping between the platform and the connecting rod, the dynamic model of the shaking table and eccentric load is shown in Fig. 3b–d. The detailed explanation of symbols is given as follows. M_T is the mass of the platform, M_L is the mass of the load, E_1 is exciter 1 of the shaking table, E_2 is exciter 2 of the shaking table, O_1 is the center of gravity of the platform, O_2 is the center of gravity of load, F_1 is the exciter force of exciter 1, F_2 is the exciter force of exciter 2, x_1 is the displacement of exciter 1, x_2 is the displacement of exciter 2, I_T is the moment of inertia of the platform relative to its own centroid axis, I_L is the moment of inertia of the load relative to its own centroid axis, M_E is the equivalent mass of the platform and load, I_E is the equivalent moment of inertia of the platform and load relative to its own centroid axis, O_E is the center of gravity of equivalent mass, x is the displacement of the equivalent mass, and ϕ is the motion angle of equivalent moment of inertia, a is the distance from the center of gravity of the equivalent mass to the center of gravity of shaking table, and l is the distance from exciter to the center of gravity of shaking table.

Figure 3c presents the dynamic model of the shaking table and eccentric load. In Fig. 3d, the shaking table and eccentric load are regarded as an integrated whole, which is an equivalent model of the dynamic model.

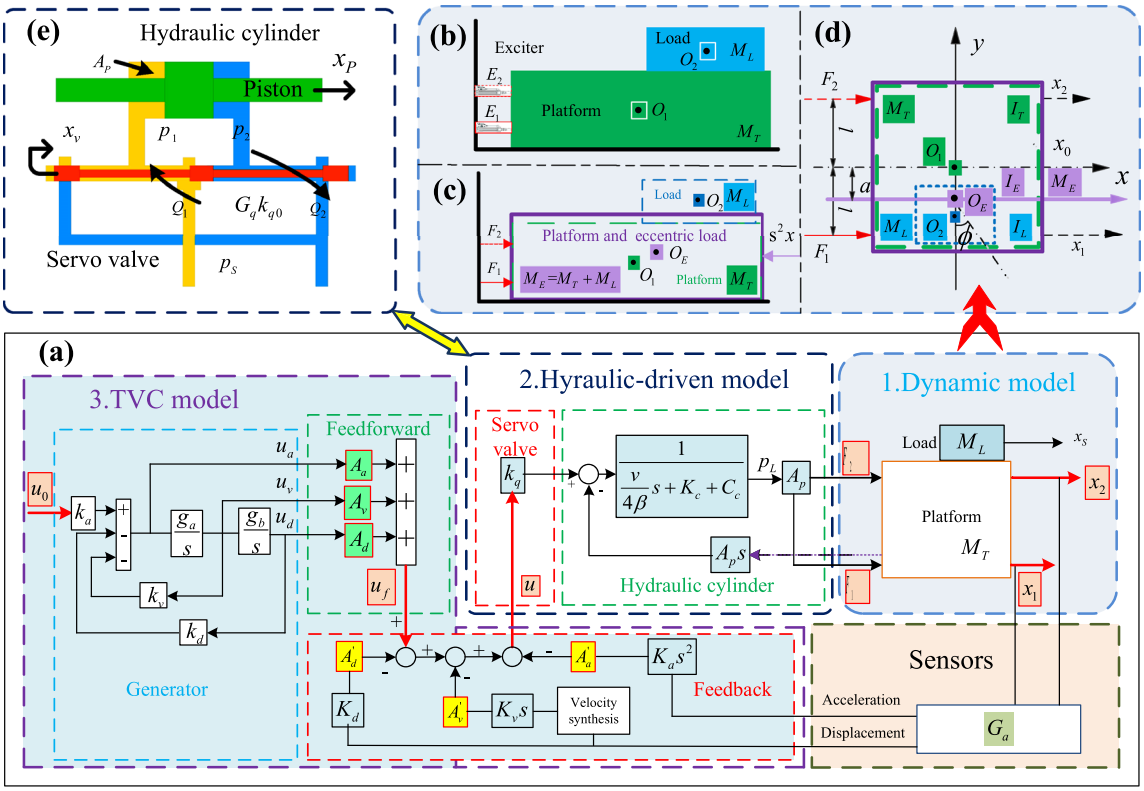

Figure 3. System modeling. (**a**) Three-sub models of the system, (**b**) dynamic model, (**c**) equivalent model of the dynamic model, (**d**) dynamic analysis of the equivalent model, and (**e**) hydraulic-driven model.

Figure 3e depicts the analysis of the mechanical properties of the equivalent model. Based on the parallel axis theorem, the equivalent model can be expressed as follows:

$$\left.\begin{aligned} M_E &= M_T + M_L \\ I_E &= I_T + I_{TA} + I_L + I_{LA} \end{aligned}\right\}, \tag{1}$$

where I_T+I_{TA} is the moment of inertia of the shaking table relative to the x-axis in Fig. 3d, I_L+I_{LA} is the moment of inertia of the load relative to the x-axis in Fig. 3d. The calculation method of the moment of inertias is given detailly in the Supplementary Materials.

Based on Eq. (1), the Newton's second law is adopted to establish the dynamic model of the shaking table and eccentric load. Then the dynamic model is

$$\left.\begin{aligned} M_E s^2 x &= F_1 + F_2 \\ I_E s^2 \phi &= F_1(l-a) - F_2(l+a) \end{aligned}\right\}. \tag{2}$$

Hydraulic-driven system modeling. The hydraulic-driven system is the driven part of the shaking table and eccentric load. The servo valve and the hydraulic cylinder are the two core components of hydraulic-driven system, the schematic diagram of which is demonstrated in Fig. 3e.

Servo valve. Generally, servo valve can be regarded as a second-order oscillation link[35], and the transfer function of servo valve is

$$k_q = G_q k_{q0} = \frac{k_{q0}}{\frac{s^2}{n_q^2} + \frac{2D_q}{n_q}s + 1}, \tag{3}$$

where k_{q0} is the flow gain of servo valve, n_q is the frequency of servo valve, and D_q is the damping ratio of servo valve.

Hydraulic cylinder. Combined with servo valve and hydraulic cylinder, the hydraulic-driven system can be expressed by a series of continuity equations[36]. The Laplace transform is applied to the continuity equations, and the converted form can be described as follows

$$\left.\begin{aligned} Q_L &= G_q k_{q0} u - K_C p_L \\ Q_L &= A_p s x_T + \frac{V}{4\beta} s p_L \\ A_p p_L &= M_{TL} s^2 x_T \end{aligned}\right\}, \tag{4}$$

where Q_L is the flow of servo valve, $G_q k_{q0}$ is the transfer function of servo valve, u is the control error signal, p_L is the load pressure, A_P is the effective area of cylinder, x_T is the displacement of the shaking table, V is the total capacity of two hydraulic cylinder chambers, β is effective bulk modulus, and M_{TL} is the total mass of load, platform and exciter piston.

TVC system modeling. The TVC model is the control part of the shaking table and eccentric load. The TVC model consists of feedback loop, feedforward loop, and generator of the TVC, the schematic diagram of which is presented in Fig. 3a.

According to the TVC system modeling process presented in Ref.[32], the control error signal is

$$u = G_3 u_0 - G_4 G_a x_T, \tag{5}$$

where u is control error signal, u_0 is control signal, G_3 is the generator and the feedforward of the TVC, G_4 is the feedback of the TVC, x_T is the displacement of shaking table, and G_a is the transfer function of sensors. The analytical expression of G_a is

$$G_a = \frac{1}{\frac{s^2}{n_a^2} + \frac{2D_a s}{n_a} + 1}, \tag{6}$$

where n_a is the frequency of sensors and D_a is the damping ratio of sensors.

Transfer function matrix modeling. The analytical transfer function matrix is established based on the three sub-models. Assuming the parameters of exciter 1 and 2 are the same, the transfer function matrix can be described as

$$\left.\begin{aligned} &\left\{\frac{G_2}{4l^2}[M_E s^2 (l+a)^2 + I_E s^2] + s\right\} x_1 + \left\{\frac{G_2}{4l^2}[M_E s^2 (l^2 - a^2) - I_E s^2]\right\} x_2 = \frac{G_q k_{q0} u_1}{A_p} \\ &\left\{\frac{G_2}{4l^2}[M_E s^2 (l-a)^2 + I_E s^2] + s\right\} x_2 + \left\{\frac{G_2}{4l^2}[M_E s^2 (l^2 - a^2) - I_E s^2]\right\} x_1 = \frac{G_q k_{q0} u_2}{A_p} \end{aligned}\right\}, \tag{7}$$

where u_1 and u_2 are the control error signals of two exciters, $G_q k_{q0}$ is the transfer function of servo valve, and the expression of G_2 is

$$G_2 = \frac{V}{4\beta A_P^2} s + \frac{K_C + C_C}{A_p^2}. \tag{8}$$

Substituting Eqs. (5), (6) and (8) into Eq. (7), the analytical transfer function matrix can be obtained as follows:

$$\left.\begin{aligned} &\left\{\frac{G_2}{4l^2}[M_E s^2 (l+a)^2 + I_E s^2] + s + \frac{G_q k_q}{A_p} G_4 G_a\right\} x_1 + \left\{\frac{G_2}{4l^2}[M_E s^2 (l^2 - a^2) - I_E s^2]\right\} x_2 = \frac{G_3 G_q k_q u_1}{A_p} \\ &\left\{\frac{G_2}{4l^2}[M_E s^2 (l-a)^2 + J_E s^2] + s + \frac{G_q k_q}{A_p} G_4 G_a\right\} x_2 + \left\{\frac{G_2}{4l^2}[M_E s^2 (l^2 - a^2) - J_E s^2]\right\} x_1 = \frac{G_3 G_q k_q u_2}{A_p} \end{aligned}\right\}. \tag{9}$$

Converting Eq. (9) into a transfer function matrix as follows:

$$\begin{Bmatrix} x_1 \\ x_2 \end{Bmatrix} = \begin{bmatrix} H_{11} & H_{12} \\ H_{21} & H_{22} \end{bmatrix} \begin{Bmatrix} u_1 \\ u_2 \end{Bmatrix}, \tag{10}$$

where H_{11} and H_{22} are the transfer function of two exciters which are affected by the CSI, H_{12} and H_{21} are the transfer functions of the coupling between two exciters, and u_1 and u_2 are the control signals of two exciters. The expressions of H_{11}, H_{12}, H_{21} and H_{22} are

$$\left.\begin{aligned} H_{11} &= \frac{G_3 G_q k_q}{A_p} \frac{G_7}{G_5 G_7 - G_6^2} \\ H_{12} = H_{21} &= \frac{G_3 G_q k_q}{A_p} \frac{-G_6}{G_5^2 - G_6^2} \\ H_{22} &= \frac{G_3 G_q k_q}{A_p} \frac{G_5}{G_5 G_7 - G_6^2} \end{aligned}\right\}, \tag{11}$$

where G_3 is the transfer function of the generator and the feedforward of the TVC. G_5, G_6, and G_7 can be written as

Conditions	MR	IR	ER
Different MR conditions	MR = 0.5	IR = 0.10	ER = 0.4
	MR = 1.0		
	MR = 1.5		
Different IR conditions	MR = 1.0	IR = 0.05	ER = 0.4
		IR = 0.10	
		IR = 0.15	
Different ER conditions	MR = 1.0	IR = 0.10	ER = 0.2
			ER = 0.4
			ER = 0.6

Table 1. Different MR, IR, and ER conditions.

$$\left.\begin{aligned} G_5 &= \frac{G_2}{4l^2}[M_E s^2(l+a)^2 + I_E s^2] + s + \frac{G_q k_q}{A_p} G_4 G_a \\ G_6 &= \frac{G_2}{4l^2}[M_E s^2(l^2 - a^2) - I_E s^2] \\ G_7 &= \frac{G_2}{4l^2}[M_E s^2(l-a)^2 + I_E s^2] + s + \frac{G_q k_q}{A_p} G_4 G_a \end{aligned}\right\}, \tag{12}$$

where G_4 is the transfer function of the feedback of the TVC, and G_a is the transfer function of sensors.

Analysis of the CSI effects

Based on the transfer function matrix, an in-depth analysis is conducted to find the sensitivity of the MR, IR, and ER to the transfer function matrix, and the influence trend and degree of the CSI effects on the transfer function matrix. The analysis is carried out under different MR, IR, and ER conditions. According to the Tables S2 and S3 in the Supplementary Materials, the different MR, IR, and ER conditions are presented in Table 1. In Table 1, the MR is denoted by MR = M_L/M_T, the IR is denoted by IR = I_L/I_T, and the ER is denoted by ER = a/l (l is 1.2 m).

For comparing and analyzing the CSI effects on the transfer function matrix, the condition that the shaking table with no load is defined as a reference condition. In the analysis, the absolute value of the amplitude frequency characteristics of H_{11} and H_{22} is taken as a quantization index. If the quantization index exceeds ± 3.00 dB, it means that the shaking table will not work in its working frequency range.

Figure 4 presents the CSI effect on the transfer function matrix under different MR, IR, and ER conditions. Figure 4a shows that at 35.60 Hz the value of H_{11} is – 3.00 dB when MR = 0.50, at 27.90 Hz the value of H_{11} is – 3.00 dB when MR = 1.0, and at 23.60 Hz the value of H_{11} is – 3.00 dB when MR = 1.50. At the same time, with the changes of the MR (from 0.5 to 1.5), the value of H_{22} remains to be – 3.00 dB at 48.60 Hz. Based on the above data, it can be obtained that at the resonance peak of oil column frequency and its surrounding frequency band, the influence of the CSI on H_{11} increases with the MR, and the MR has no obvious effect on H_{22}. Besides, the frequency of the resonance peak of oil column of H_{11} decreases with the MR, and the value of the resonance peak of oil column of H_{11} increases with the MR. It can be observed from Fig. 4b that at 10.00 Hz, the value of H_{12} and H_{21} is – 49.40 dB under the reference condition, but it is – 32.10 dB when MR = 0.5, – 23.10 dB when MR = 1.0, and – 18.00 dB when MR = 1.5. According to these collected data, it can be concluded that with the increase of the MR, the coupling between two exciters increases rapidly. The coupling is amplified at least 31.40 dB (about 37.15 times).

Figure 4c shows that although the value of the IR changes, the values of H_{11} are – 3.00 dB at 27.95 Hz and 3.21 dB at 15.90 Hz, and the values of H_{22} are – 0.72 dB at 34.70 Hz. Figure 4d illustrates the fact that although the IR conditions are different, both of the values of H_{12} and H_{21} are 23.80 dB at 10.00 Hz. Based on the above data, it can be drawn that the IR only has a slight effect (the quantization index does not exceed ± 1.00 dB) on H_{12} and H_{21} when the frequency exceeds 40.00 Hz. The sensitivity of the IR to each transfer function in the transfer function matrix is low.

Figure 4e shows that at 30.00 Hz, the value of H_{11} is – 3.00 dB when ER = 0.2, at 27.90 Hz the value of H_{11} is – 3.00 dB when ER = 0.4, at 26.30 Hz the value of H_{11} is – 3.00 dB when ER = 0.6, and at 15.60 Hz the value of H_{11} is 3.93 dB when ER = 0.6. Meanwhile, at 42.20 Hz the value of H_{22} is – 3.00 dB when ER = 0.2, at 47.20 Hz the value of H_{22} is – 3.00 dB when ER = 0.4, and at 50.20 Hz the value of H_{22} is – 3.00 dB when ER = 0.6. According to the data collected, it can be obtained that at the resonance peak of oil column frequency and its surrounding frequency band, the influence of the CSI on H_{11} increases with the ER, and the influence of the CSI on H_{22} decreases with the ER. Meanwhile, the frequency of the resonance peak of oil column of H_{11} decreases with the ER, and the value of the resonance peak of oil column of H_{11} increases with the ER. Besides, the effective frequency band of H_{22} increases at a certain extent, but the frequency does not exceed the effective frequency band of the reference condition. It can be observed from Fig. 4f that at 10.00 Hz, the values of both H_{12} and H_{21} are – 21.90 dB when ER = 0.2, – 23.20 dB when ER = 0.4, and – 25.80 dB when ER = 0.6. These data show that the coupling between the two exciters decreases with the ER.

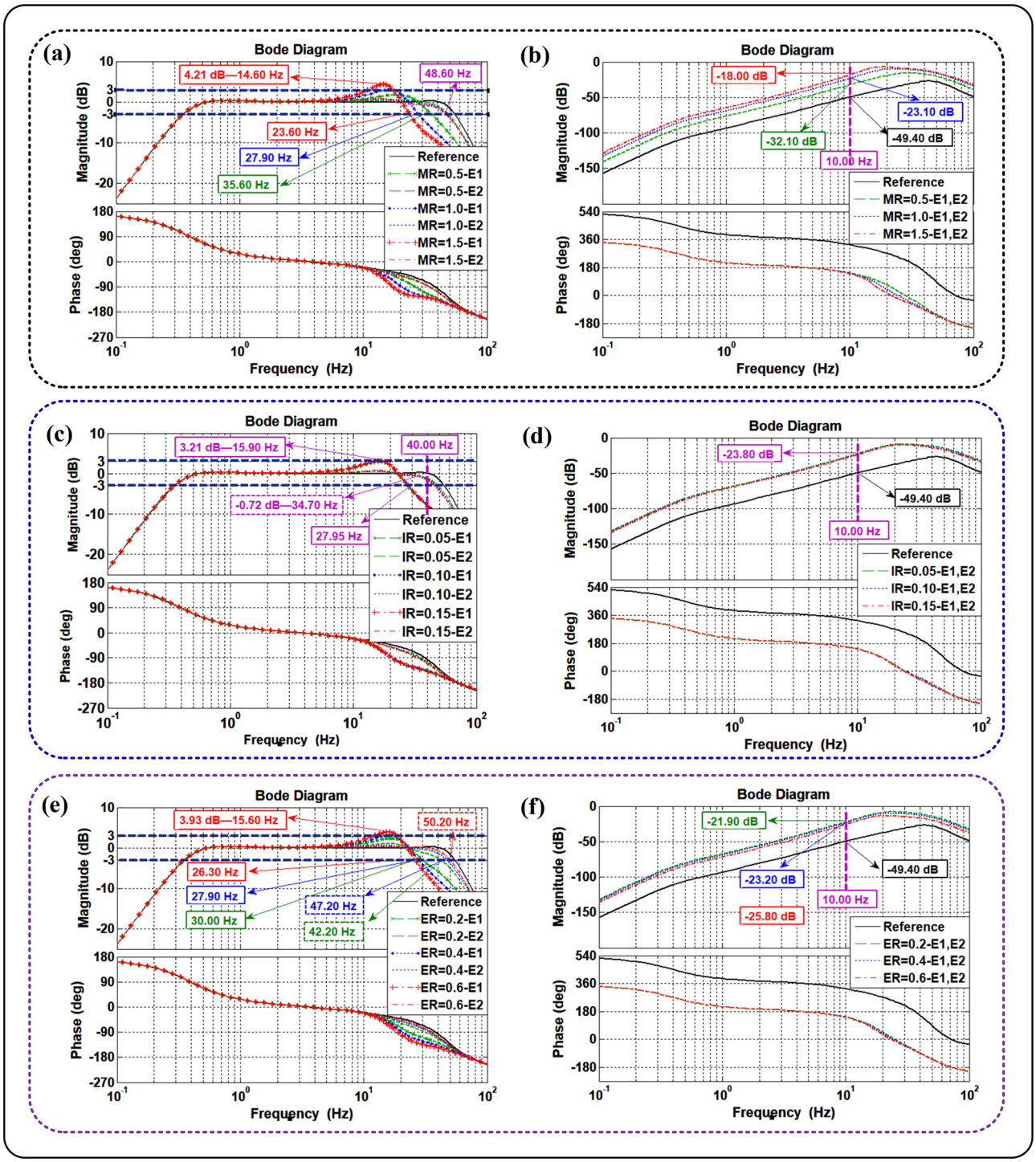

Figure 4. CSI effects on the transfer function matrix. (**a**) Effects of MR on H_{11} and H_{22}, (**b**) effects of MR on H_{12} and H_{21}, (**c**) effects of IR on H_{11} and H_{22}, (**d**) effects of IR on H_{12} and H_{21}, (**e**) effects of ER on H_{11} and H_{22}, and (**f**) effects of ER on H_{12} and H_{21} (E1 and E2 are the two exciters of shaking table).

According to Fig. 4, the MR, ER, and IR have no evident effect on the phase diagram of the transfer function matrix (the quantization index does not exceed ± 60°), and thus, the phase diagram is not discussed in this paper. Besides, the role of the ER can be identified as follows. The ER exerts effects on the transfer function matrix at the resonance peak of oil column frequency and its surrounding frequency band.

Assessment of the CSI effects

The above "Analysis of the CSI effects" proves that the CSI exerts different degrees of effects on the transfer function matrix. However, the above analysis needs to be further expanded to appraise the CSI effect in practical experiments. To appraise whether the CSI effects can be ignored in shaking table test, a novelty effect assessment is proposed. Two steps are involved in proposing the assessment. The first step is the deduction of the assessment, and the second step is the visualization expression of the assessment.

Deduction of the effect assessment. The "Analysis of the CSI effects" proves that the MR, IR, and ER have influence on the H_{11} and H_{22}. In the light of Eq. (1) and the parallel axis theorem, the MR, IR, and ER are related to the mass and the inertia moment of the system. The relationship indicates that the CSI effects are related to two physical quantities, the moment of inertia and the mass of the system. In the deduction of the effect assessment, the ratio of the moment of inertia of shaking table to the moment of inertia of the system (IRS) and the MR are adopted to represent the two physical quantities.

It is assumed that the assessment can be expressed as follows:

$$CSI(IRS) = f_1(IR, ER, MR), \tag{13}$$

$$CSI(MR) = f_2(MR), \tag{14}$$

where IRS is the ratio of the I_T to the I_E, and the expression of IRS is

$$IRS = \frac{I_T}{I_E} = \frac{I_T}{I_T + I_{TA} + I_L + I_{LA}}. \tag{15}$$

Referring to the expressions of I_T, I_{TA}, I_L, and I_{LA} in Supplementary Materials, Eq. (13) can be written as

$$CSI(IRS) = f_1\left(\frac{(m^2+n^2)\cdot M_T}{\begin{array}{l}(m^2+n^2)\cdot M_T + 12\cdot M_T\cdot(\frac{M_L}{M_T+M_L}A)^2\\ +(c^2+k^2)\cdot M_L + 12\cdot M_L\cdot(\frac{M_T}{M_T+M_L}A)^2\end{array}}\right), \tag{16}$$

where m and n are the length and the width of the shaking table, respectively. c and k are the length and the width of the load, respectively. And A is the distance from the center of gravity of the load to the center line of shaking table.

Employing $MR = M_L/M_T$, Eq. (16) can be expressed more compactly as

$$CSI(IRS) = f_1\left(\frac{m^2+n^2}{\begin{array}{l}m^2+n^2+(c^2+k^2)\cdot MR\\ +12\cdot a^2\cdot MR/(1+MR)\end{array}}\right). \tag{17}$$

According to $ER = a/l$, Eq. (17) can be conveniently transformed into

$$CSI(IRS) = f_1\left(\frac{m^2+n^2}{\begin{array}{l}m^2+n^2+(c^2+k^2)\cdot MR\\ +12\cdot ER^2\cdot l^2\cdot MR/(1+MR)\end{array}}\right). \tag{18}$$

Finally, Eq. (13) can be obtained as follows:

$$CSI(IRS) = f_1\left(\frac{1}{1+IR+12\cdot ER^2\cdot\frac{l^2}{(m^2+n^2)}\cdot\frac{MR}{1+MR}}\right). \tag{19}$$

With the combination of Eq. (14), the assessment can be described as follows:

$$\left.\begin{array}{l}CSI(IRS) = f_1\left(\frac{1}{1+IR+12\cdot ER^2\cdot\frac{l^2}{(m^2+n^2)}\cdot\frac{MR}{1+MR}}\right)\\ CSI(MR) = f_2(MR)\end{array}\right\}. \tag{20}$$

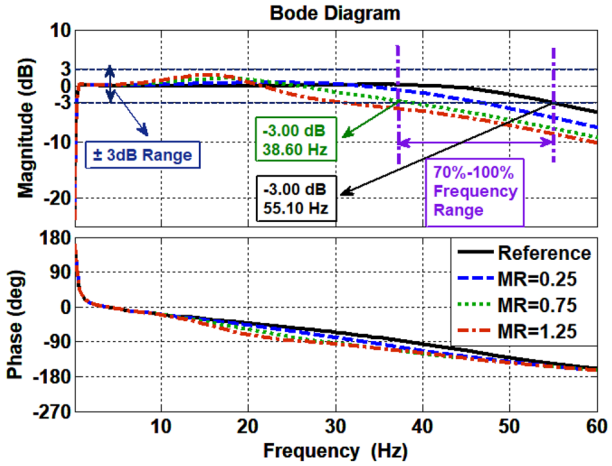

Figure 5. Determination of the MR.

Visualization expression of the effect assessment. For the convenient application of the assessment, Eq. (20) is simplified and visualized as follows. According to the conclusion in "Analysis of the CSI effects" that the changes of the IR have slight effect on the transfer function matrix. If the IR is set to be 0.1 (the value of IR is determined according to the characteristics of load in Table S2 in the Supplementary Materials), then Eq. (20) can be simplified as

$$\left.\begin{aligned} CSI(IRS) &= f_1\left(\frac{1}{1.1+12\cdot ER^2\cdot\frac{l^2}{(m^2+n^2)}\cdot\frac{MR}{1+MR}}\right)\\ CSI(MR) &= f_2(MR)\end{aligned}\right\}. \tag{21}$$

Referring to the basic characteristics of the shaking table in Table S3 in the Supplementary Materials, then Eq. (21) can be expressed as

$$\left.\begin{aligned} CSI(IRS) &= f_1\left(\frac{1}{1.1+0.96\cdot ER^2\cdot\frac{MR}{1+MR}}\right)\\ CSI(MR) &= f_2(MR)\end{aligned}\right\}. \tag{22}$$

It can be analyzed from Eq. (22) that the CSI effects are related to the MR and ER. Based on the analysis, a visualization expression of the assessment can be obtained. The concept for obtaining the visualization expression is presented as follows. Firstly, to appraise whether the CSI effects can be ignored, a judgment standard needs to be proposed. The standard is that if the amplitude characteristics of H_{11} and H_{22} exceed the range of ± 3.00 dB or the effective frequency band of H_{11} and H_{22} decreases to 70% of the frequency band of the reference condition, the CSI effects cannot be ignored. Secondly, the values of the MR and ER are determined according to the standard. In the determination process, the range of the MR is investigated under the assumption of ER = 0, and then the ER is obtained under specific value of MR.

According to the concept, the characteristics of the H_{11} and H_{22} under different MR are determined. The result of the determination is presented in Fig. 5. It can be seen from Fig. 5 that when MR = 0.75 the values of H_{11} and H_{22} are both − 3.00 dB at 38.60 Hz, which just meets the judgment standard. It can be concluded that the MR ≤ 0.75.

Based on the conclusion that the MR ≤ 0.75, the specific values of MR, − 0.75, 0.60, 0.45, and 0.30, are adopted to obtain the values of the ER. Then the coordinate points (MR, ER) are drawn in rectangular coordinate system, and a curve can be obtained by connecting the points (MR, ER). The curve is the visualization expression of the assessment of which is shown Fig. 6. To illustrate the specific meaning of the coordinate points, the point (0.45, 0.0875) is taken as an example. The point (0.45, 0.0875) indicates that when MR = 0.45, the CSI effects can be ignored if ER ≤ 0.0875. If a point (MR, ER) is above the curve, the CSI cannot be ignored, and if a point (MR, ER) is below the curve, then the CSI can be ignored.

Conclusions

In this study, an analytical transfer function matrix is established to analyze the CSI effects between the twin-axes shaking table and eccentric load. Based on the transfer function matrix, a comprehensive investigation is conducted under different MR, IR, and ER conditions. The sensitivities of the MR, IR, and ER to the transfer function matrix, the influence frequency range and the influence trend of the CSI effects are obtained. Furthermore, a novelty effect assessment is proposed to appraise whether the CSI effects can be ignored in shaking table test. The most important conclusions can be drawn as follows.

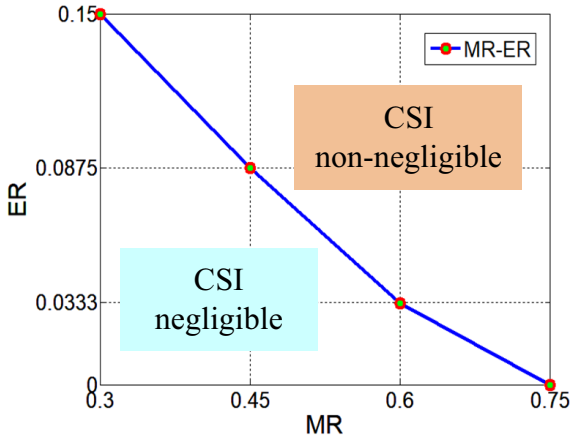

Figure 6. Visualization expression of the assessment.

(1) The ER exerts effects on the transfer function matrix at the resonance peak of oil column frequency and its surrounding frequency band.
(2) The transfer function matrix is the most sensitive to the changes of the MR, followed by the ER and then the IR. The IR has slight influence on the transfer function matrix. Additionally, the CSI exerts different influence trend and the influence degree on the transfer function matrix under different MR, ER, and IR conditions.
(3) The CSI leads to a significant increase in the exciter coupling. The coupling between two exciters is amplified at least 37.15 times.
(4) The novelty effect assessment has a wide application prospect and practical value in appraising whether the CSI effects can be ignored in shaking table test.
(5) It is worth expanding the assessment to appraise the CSI effect between shaking table and flexible structure in the future.

Data availability

All data is available in the main text or the Supplementary Information. The data are available from the corresponding author upon reasonable request.

Received: 26 April 2022; Accepted: 2 September 2022
Published online: 12 September 2022

References

1. Krinsley, D. & Takahashi, T. Surface textures of sand grains: An application of electron microscopy. *Science* **135**(3507), 923–925 (1962).
2. Ji, F., Wang, B. & Zhang, L. Light-triggered catalytic performance enhancement using magnetic nanomotor ensembles. *Research* **2020**, 6380794 (2020).
3. Beuel, A. K. *et al.* LEDitshake: A lighting system to optimize the secondary metabolite content of plant cell suspension cultures. *Sci. Rep.* **11**, 23353 (2021).
4. Severn, R. T. The development of shaking tables—A historical note. *Earthq. Eng. Struct. Dyn.* **40**(2), 195–213 (2011).
5. Zhou, T. *et al.* Shaking table tests on seismic response of discontinuous suspended ceilings. *J. Build. Eng.* **43**, 102916 (2021).
6. Blondet, M., Tarque, N., Ginocchio, F. & Villa-García, G. Shaking table testing of adobe masonry structures. In *Structural Characterization and Seismic Retrofitting of Adobe Constructions. Building Pathology and Rehabilitation* (eds Varum, H. *et al.*) 121–151 (Springer, 2021).
7. He, Y., Wang, Z. & Zhang, Y. The electromagnetic separation system for the small spherical satellite Q-SAT. *Acta Astronaut.* **184**, 180–192 (2021).
8. Su, W. & Song, W. A real-time hybrid aeroelastic simulation platform for flexible wings. *Aerosp. Sci. Technol.* **95**, 105513 (2019).
9. Plummer, R. A. Control techniques for structural testing: A review. *Proc. Inst. M. Eng. I J. Syst. Control Eng.* **221**(2), 139–169 (2007).
10. Dursun, U., Cansever, G. & Üstoğlu, İ. Neuro-fuzzy iterative learning control for 4-poster test rig. *Trans. Inst. Meas. Control.* **42**(12), 2262–2275 (2020).
11. Dyke, S. J., Spencer, B. F. Jr., Quast, P. & Sain, M. K. The role of control-structure interaction in protective system design. *J. Eng. Mech.* **121**(2), 322–338 (1995).
12. Battaini, M., Yang, G. & Spencer, B. F. Bench-scale experiment for structural control. *J. Eng. Mech.* **126**(2), 140–148 (2000).
13. Venanzi, I., Ierimonti, L. & Ubertini, F. Effect of control-structure interaction in active mass driver systems with electric torsional servomotor for seismic applications. *Bull. Earthq. Eng.* **15**, 1543–1557 (2017).
14. Zhao, J. *et al.* Modal space three-state feedback control for electro-hydraulic servo plane redundant driving mechanism with eccentric load decoupling. *ISA Trans.* **77**, 201–221 (2018).
15. Najafi, A. & Spencer, B. F. Modified model-based control of shake tables for online acceleration tracking. *Earthq. Eng. Struct. Dyn.* **49**(15), 1721–1737 (2020).
16. Ryu, K. P. & Reinhorn, A. M. Real-time control of shake tables for nonlinear hysteretic systems. *Struct. Control Health* **24**(2), 1871 (2016).

17. Blondet, M. & Esparza, C. Analysis of shaking table-structure interaction effects during seismic simulation tests. *Earthq. Eng. Struct. Dyn.* **16**(4), 473–490 (1988).
18. Wang, J., Li, X., Li, F. & Zhang, B. Effect and compensation of the interaction between a unidirectional twin-axis shaking table and the tested structure. *J. Vib. Shock* **40**(10), 140–149 (2021).
19. Conte, J. P. & Trombetti, T. L. Linear dynamic modeling of a uni-axial servo-hydraulic shaking table system. *Earthq. Eng. Struct. Dyn.* **29**(9), 1375–1404 (2000).
20. Trombetti, T. L. & Conte, J. P. Shaking table dynamics: Results from a test-analysis comparison study. *J. Eng. Mech.* **6**(4), 513–551 (2002).
21. Chen, S. *Study on Multi DOF Elastic Load Modeling of Electro-hydraulic Servo Shaking Table* (Harbin Engineering University, 2017).
22. Huang, H. H. *Design and Application of the Shaking Table* (Seismological Press, 2008).
23. Tang, Z., Li, Z., Zhou, D., Ji, J. & Ma, H. The effects on the earthquake simulation caused by the characteristics of the specimen in the shaking table tests—Part 2: The effects on the replaying precision of the recorded seismic waves and the real-time compensation. *J. Beijing Univ. Technol.* **36**(9), 1199–1205 (2010).
24. Guo, W. *et al.* Accuracy assessment of shake table device on strong earthquake output. *Adv. Civ. Eng.* **2019**, 1–23 (2019).
25. Li, Z., Tang, Z., Zhou, D., Ji, J. & Ma, H. The effects on the earthquake simulation caused by the characteristics of the specimen in the shaking table tests-part 1: The effects on the stability of the system. *J. Beijing Univ. Technol.* **36**(8), 1091–1098 (2010).
26. Zhang, L. *Research on Time Waveform Replication Control Strategy of Redundant-Driven Electro-hydraulic Shaking Tables* (Harbin Institute of Technology, 2017).
27. Yan, F. *Structural Optimization and Control Study of Electro-hydraulic Servo Planar Redundant Mechanism* (Harbin Institute of Technology, 2015).
28. Xie, Z. *Decoupling Control for Multi-axis Seismic Testing Table Based on the Dynamic Model* (Harbin Institute of Technology, 2017).
29. Maoult, A. L., Queval, J. C. & Bairrao, R. Dynamic interaction between the shaking table and the specimen during seismic tests. In *Advances in Performance-Based Earthquake Engineering* (ed. Fardis, M.) 431–440 (Springer, 2010).
30. Wang, J. *Research on Time Waveform Replication Control Strategy of the Systems of Shaking Table/Multiple Shaking Tables Array and Test Structure* (Beijing University of Technology, 2020).
31. Li, F., Li, X. & Wang, J. Effects of interaction between dual shaking tables and specimen and force feedback compensation control. *Shock. Vib.* **2018**, 1–12 (2018).
32. Wang, J., Li, X., Li, F. & Li, N. Analysis of the interaction effects between double shaking tables and test structure. *J. Vib. Control* **27**(11–12), 1407–1419 (2021).
33. Zhao, J. *et al.* Modal space three-state feedback and feedforward control for 2-DOF electro-hydraulic servo shaking table with dynamic coupling caused by eccentric load. *Mechatronics* **79**, 102661 (2021).
34. Guo, W. *et al.* Facility performance indexes and rapid test feasibility evaluation method of shaking tables. *Ksce J. Civ. Eng.* **23**(7), 3097–3112 (2019).
35. Wang, J. *et al.* Differential movement synchronous tracking control strategy of double-shaking table system loading with specimen. *Shock. Vib.* **2018**, 1–11 (2018).
36. Dai, K. *et al.* Adaptive force tracking control of electrohydraulic systems with low load using the modified LuGre friction model. *Control Eng. Pract.* **125**(11), 105213 (2022).

Acknowledgements

The National Natural Science Foundation of China (51978015), the China Postdoctoral Science Foundation (2021M692972), the Special Fund of the Institute of Geophysics, China Earthquake Administration (DQJB22X09 and DQJB20K45), and the Opening Project of the Key Laboratory of the Beijing University of Technology (2021B01) supported this work.

Author contributions

X.L., J.J. and J.W. conceptualized the idea and established the analytical model. Z.Z. and S.C. conducted methodology of the assessment criteria. J.W. and A.L. designed the analysis of the CSI effect conditions and analyzed data. S.C. and A.L. contributed to conducting simulation, analyzing results and interpreting data. A.L. and X.L. directed the research. All authors contributed to the analysis of the results and edited the manuscript.

Competing interests

The authors declare no competing interests.

Additional information

Supplementary Information The online version contains supplementary material available at https://doi.org/10.1038/s41598-022-19743-y.

Correspondence and requests for materials should be addressed to X.L.